PLOS ONE

RESEARCH ARTICLE

Side-by-side comparison of published small molecule inhibitors against thapsigargin-induced store-operated Ca^{2+} entry in HEK293 cells

Katherine Norman[1,2], Karen E. Hemmings[2], Heba Shawer[2], Hollie L. Appleby[2], Alan J. Burnett[2], Nurasyikin Hamzah[1], Rajendra Gosain[2], Emily M. Woodhouse[2], David J. Beech[2], Richard Foster[1,2], Marc A. Bailey[2]*

1 School of Chemistry, University of Leeds, Leeds, West Yorkshire, United Kingdom, **2** Discovery and Translational Science Department, Leeds Institute of Cardiovascular and Metabolic Medicine, School of Medicine, University of Leeds, Leeds, West Yorkshire, United Kingdom

* m.a.bailey@leeds.ac.uk

Citation: Norman K, Hemmings KE, Shawer H, Appleby HL, Burnett AJ, Hamzah N, et al. (2024) Side-by-side comparison of published small molecule inhibitors against thapsigargin-induced store-operated Ca^{2+} entry in HEK293 cells. PLoS ONE 19(1): e0296065. https://doi.org/10.1371/journal.pone.0296065

Editor: Alexander G. Obukhov, Indiana University School of Medicine, UNITED STATES

Received: May 12, 2023

Accepted: December 5, 2023

Published: January 23, 2024

Data Availability Statement: All relevant data are within the paper and its Supporting Information files.

Funding: This work was supported by an Medical Research Council studentship (MR/N013840/1) https://www.ukri.org/councils/mrc/ to K.N., a British Heart Foundation PhD studentship (FS/17/66/33480) https://www.bhf.org.uk/ to H.S., a British Heart Foundation PhD studentship to H.L.A. (FS/13/23/30122), a British Heart Foundation PhD

Abstract

Calcium (Ca^{2+}) is a key second messenger in eukaryotes, with store-operated Ca^{2+} entry (SOCE) being the main source of Ca^{2+} influx into non-excitable cells. ORAI1 is a highly Ca^{2+}-selective plasma membrane channel that encodes SOCE. It is ubiquitously expressed in mammals and has been implicated in numerous diseases, including cardiovascular disease and cancer. A number of small molecules have been identified as inhibitors of SOCE with a variety of potential therapeutic uses proposed and validated *in vitro* and *in vivo*. These encompass both nonselective Ca^{2+} channel inhibitors and targeted selective inhibitors of SOCE. Inhibition of SOCE can be quantified both directly and indirectly with a variety of assay setups, making an accurate comparison of the activity of different SOCE inhibitors challenging. We have used a fluorescence based Ca^{2+} addback assay in native HEK293 cells to generate dose-response data for many published SOCE inhibitors. We were able to directly compare potency. Most compounds were validated with only minor and expected variations in potency, but some were not. This could be due to differences in assay setup relating to the mechanism of action of the inhibitors and highlights the value of a singular approach to compare these compounds, as well as the general need for biorthogonal validation of novel bioactive compounds. The compounds observed to be the most potent against SOCE in our study were: 7-azaindole 14d (12), JPIII (17), Synta-66 (6), Pyr 3 (5), GSK5503A (8), CM4620 (14) and RO2959 (7). These represent the most promising candidates for future development of SOCE inhibitors for therapeutic use.

Introduction

The calcium (Ca^{2+}) ion is involved in key cellular processes including signalling, mitochondrial regulation, motility and apoptosis. It is typically found at ~100 nM intracellular free

studentship to EMW (FS/16/42/32308) a British Heart Foundation fellowship (FS/18/12/33270 and FS/12/54/29671) to MAB and DJB and a Medical Research Council Confidence in Concept grant (MC PC 14109) to M.A.B., R.F. and D.J.B. The funders had no role in study design, data collection and analysis, decision to publish, or preparation of the manuscript.

Competing interests: The authors have declared no competing interests exist.

concentration and ~2 mM extracellularly, a ~20,000× difference [1]. The main source of Ca^{2+} influx into non-excitable cells is store-operated (or capacitative) Ca^{2+} entry (SOCE), in which eukaryotic cells store Ca^{2+} in the endoplasmic reticulum (ER), using sarco-/endoplasmic reticulum Ca^{2+} ATPase (SERCA) pumps to counteract the continual leakage back into the cytoplasm. If the SERCA pump is blocked, or during a signalling event, the ER Ca^{2+} stores will deplete, and SOCE is activated. This model of Ca^{2+} influx was first proposed in 1986 [2], and the resulting current, known as the Ca^{2+}-release activated Ca^{2+} current (I_{CRAC}), was identified in 1997 [3]. ORAI1 is the pore-forming plasma membrane (PM) protein subunit of the CRAC channel encoding SOCE. It was identified in 2006 [4–6] and has three mammalian homologs, ORAI1, ORAI2, and ORAI3. They share no close homology with any known proteins [7]. The ER membrane (EM) protein stromal interaction molecule 1 (STIM1) was identified in 2005 as a transmembrane ER Ca^{2+}-sensor [8]. STIM1 units cluster forming punctae with ORAI1 opening the channel pore allowing Ca^{2+} influx into the cytosol allowing ER store refilling [9]. The X-ray crystal structure of *Drosophila melanogaster* ORAI1, (73% sequence homology with humans) was solved in 2012 to a 3.35 Å resolution [10] revealing four transmembrane domains and a hexamer about the pore and supported by recent functional and cryo-EM structural data [11–13].

Loss-of-function mutations in ORAI1 and STIM1 are associated with immunodeficiency [14–16], autoimmunity [17], muscle hypotonia [18,19] and dental enamel defects [20]. Whilst gain-of-function mutations have been linked to platelet disorders [21] and myopathy [22]. Much research has focused on ORAI1 and SOCE as a drug target in immunology and inflammatory disease [23–26]. However, a growing body of evidence links SOCE/ORAI1 to cardiovascular and cardiorespiratory pathologies [27–30]. Small molecule inhibition of SOCE and genetic disruption of *Orai1* using a dominant negative mutant (in cardiac myocytes) was cardioprotective following pressure overload heart failure induction [31]. Both ORAI1 and ORAI2 are upregulated in pulmonary arterial smooth muscle cells (PASMCs) under hypoxic conditions and so could prove therapeutic targets for hypoxia-induced pulmonary hypertension [32]. SOCE and basal [Ca^{2+}] are increased in high fat-fed apolipoprotein E-knockout mice, which have elevated blood lipids but no atherosclerotic plaques [33], and ORAI1 knockdown or chemical inhibition reduced atherosclerotic plaque size in this model [34] suggesting a potential therapeutic role to treat atherosclerosis and neointimal hyperplasia [35,36]. SOCE in platelets is required for thrombus formation [37] making it a target for the development of antithrombotic drugs [38,39]. Several small molecule SOCE inhibitors have been shown to reduce thrombus formation in whole blood, and 2-APB reduced thrombus formation in a murine stroke model [40]. These are thought to function by inhibition at ORAI1, although this remains to be definitively proven. Other potential therapeutic targets for SOCE inhibitors include skeletal muscle diseases [41], cancers [42–44], neurology and pain [45–48] and secretory epithelial cell disorders [49–51]. Although none are currently licensed for clinical use, a number have reached clinical trials for conditions including acute pancreatitis and COVID-19-associated pneumonia [52–54]. The success of these compounds in reaching clinical trials highlights the plausibility of SOCE inhibition as a safe therapeutic strategy in humans.

While the potencies of several SOCE inhibitors are published, they have been studied by different research groups/companies using different experimental approaches and cell lines for assessment. A direct comparison between the literature compounds using a single assay and a non-disease specific cell line is lacking. The existing SOCE inhibitors have been reviewed extensively and recently [36,55–59]. Here we report a direct comparison of the published SOCE small molecule inhibitors (presented in S1 Fig) using a fluorescence based Ca^{2+} recording system to measure thapsigargin (TG) induced SOCE in Human Embryonic Kidney 293 (HEK293) cells. These Ca^{2+} events were measured with Fura-2, a ratiometric dye that is a

popular tool for the study of Ca^{2+} events due to its brightness, resistance to photobleaching, high affinity for Ca^{2+}, and its selectivity over other divalent cations [60,61]. Thapsigargin, a widely used natural SERCA pump inhibitor with high potency and selectivity, was used to deplete the ER Ca^{2+} stores in the absence of extracellular Ca^{2+}, before extracellular Ca^{2+} was added back, triggering SOCE [62,63]. HEK293 cells are frequently used for the initial assessment of SOCE inhibitors. Recent studies in which knock-out of ORAI1, 2 or 3 either alone or in combination have clearly demonstrated ORAI1 to be the main store-operated channel in this cell line [64,65] making it an excellent model system for screening compounds with potential for therapeutic use.

Materials and methods

Cell culture

HEK293 cells (CRL-1573, ATCC, Teddington, UK) were maintained in Dulbecco's Modified Eagle's Medium (DMEM, Gibco, Thermo Fisher Scientific, UK) supplemented with 10% fetal bovine serum (FBS, Gibco, Thermo Fisher Scientific, UK) and 100 unit mL-1 penicillin-streptomycin (Gibco, Thermo Fisher Scientific, UK) at 37˚C in a humidified 5% CO_2 incubator. Cells were grown to 95% confluence before passage and utilised at 95% confluence for experiments. Cells were used up to passage number ~30 before being discarded.

Chemicals

All chemicals and solvents were used as supplied. SKF96365 (1), CAI (2), 2-APB (3), Pyr2 (4), Pyr3 (5), Synta-66 (6), RO2959 (7) AnCoA4 (10), leflunomide (15), $Gd^{3+,}$ (18) and La^{3+} (19) were purchased from Sigma-Aldrich (UK). CM4620 (14) was purchased from MedChemExpress (Insight Biotechnology Ltd, UK). Teriflunomide (16) was purchased from APExBIO (UK). MRS1845 (11) was purchased from Santa Cruz Biotechnology (Insight Biotechnology Ltd, UK). Compounds that were not commercially available were synthesised. CM3457 (13) was synthesised by Dr Rajendra Gosain (unpublished). JPIII (17) was synthesised as previously reported [31]. The synthetic route for GSK7975A (9) and GSK5503A (8) largely followed the patent protocol and is summarised in S2 and S3 Figs, respectively [66]. Synthesis of the 7-azaindole series compound (12) (S4 Fig) loosely followed the patent protocol [67]. Detailed chemistry methods for compound syntheses can be found in S1 Appendix and NMR data for all compounds and intermediates synthesized can be found in S5–S17 Figs.

Fura-2 Ca^{2+} addback assay

Fluorescence measurements were recorded using a FlexStation III (Molecular Devices Limited, UK), running software Softmax Pro version 4.7.1 or 7.0.3. HEK293 cells were seeded onto Cellcoat Poly-D-Lysine 96-well plates (Greiner, UK) at a seeding density of 60,000 cells per well and incubated overnight at 37˚C in a 5% CO_2 incubator. The Ca^{2+} addback protocol used here followed published protocols [31,68,69]. Briefly, cells were incubated in 1.5 mM Ca^{2+} SBS (standard bath solution, NaCl 135 mM, KCl 5 mM, $MgCl_2$ 1.2 mM, Glucose 8 mM, HEPES 10mM, $CaCl_2$ 1.5 mM, pH 7.4) containing Fura-2AM (Molecular Probes, Thermo Fisher Scientific, UK) (2 μM) and 0.01% pluronic acid (in DMSO) for 1 hour at 37˚C in the dark and then washed with 1.5 mM Ca^{2+} SBS. Thapsigargin (Sigma, UK) (1 μM) and test compound (concentrations below) or vehicle in 0 mM Ca^{2+} SBS (NaCl 135 mM, KCl 5 mM, $MgCl_2$ 1.2 mM, glucose 8 mM, HEPES 10 mM, EGTA 0.4 mM, pH 7.4) were added and the cells incubated for a further 30 minutes at room temperature in the dark. Afterwards, 1.5 mM Ca^{2+} SBS, also containing test compound at the same concentration as the pre-treatment, was added to

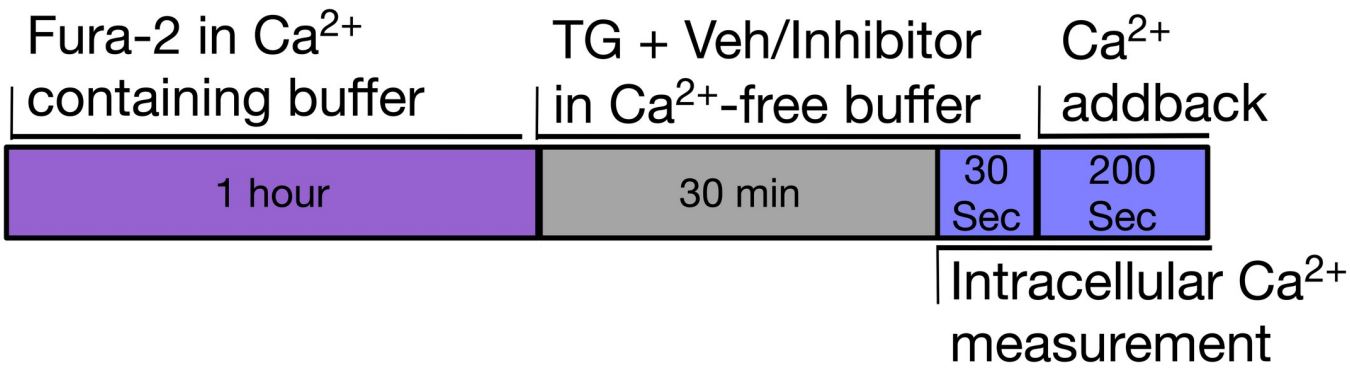

Fig 1. A time series schematic for the Ca^{2+} addback protocol.

https://doi.org/10.1371/journal.pone.0296065.g001

enable SOCE upon Ca^{2+} addback (0.3 mM final Ca^{2+} addback concentration after the 1:5 dilution). The 0.3 mM Ca^{2+} addback concentration was selected based on the demonstration that subtle changes in SOCE may be masked when higher Ca^{2+} addback concentrations are used [4]. Fluorescence measurements were recorded every 5 seconds for 200 seconds using 340/380 nm excitation wavelength and 510 nm emission. A schematic of this process is shown in Fig 1. AnCoA4 (10) and MRS1845 (11), were also tested with a longer exposure to compound, via inclusion of compound during the 1 hour Fura-2 loading step, such that a total exposure time of 90 mins was tested to determine whether a longer preincubation improved potency.

Calculations and statistics

The ratio between excitation at 340 nm and 380 nm was calculated at each timepoint ($\Delta F^{340/380}$). The mean of the first three readings was used as the baseline and subtracted from each value to calculate the baseline corrected $\Delta F^{340/380}$. The IC_{50} curves were calculated using the peak baseline corrected $\Delta F^{340/380}$ at concentrations of 0.1 nM, 1 nM, 10 nM, 100 nM, 1 μM and 10 μM [compound] after subtraction of the no TG control peak value. Values were then normalized to the vehicle containing TG and a modified Hill equation was fitted to the data. The exceptions to this (where literature indicated that the standard concentration range would be inappropriate due to reduced compound potency) were: SKF96365 (1) and AnCoA4 (10) (assessed at 2.5, 5, 10, 20, 40 and 80 μM); Carboxyamidotriazole (2) (assessed at 2 nM, 20 nM, 200 nM, 2 μM, 10 μM and 20 μM); 2-APB (3) (assessed at 5, 10, 25, 33, 66, and 100 μM); MRS1845 (11) (assessed at 1 nM, 10 nM, 100 nM, 1 μM, 10 μM and 50 μM); CM4620 (14) (assessed at 0.1 nM, 1 nM, 10 nM, 100 nM, 1 μM and 5 μM); leflunomide (15) (assessed at 10, 100, 200, 300, 400 and 500 μM); teriflunomide (16) (assessed at 10, 50, 100, 200, 300 and 400 μM); JPIII (17) (assessed at 20 nM, 70 nM, 300 nM, 1.25 μM, 5 μM and 20 μM). A DMSO concentration of 0.1% v/v was consistent in all solutions. The mean ± SD was calculated from three independent experiments (n = 3), with each condition tested in triplicate for each experiment (N = 3/n = 3). To perform a comparison of SOCE inhibitory activity the % vehicle of each inhibitor at 10 μM was analyzed using an ANOVA one-way test with Dunnett's post-hoc test using GraphPad Prism 9.0. A p value < 0.05 was considered significant.

Results

Evaluation of the SOCE inhibitors in HEK293 cells

The TG induced SOCE method was used to monitor $\Delta F^{340/380}$ fluorescence over time as a proxy for intracellular Ca^{2+} concentration (Fig 2) and used to generate dose response curves

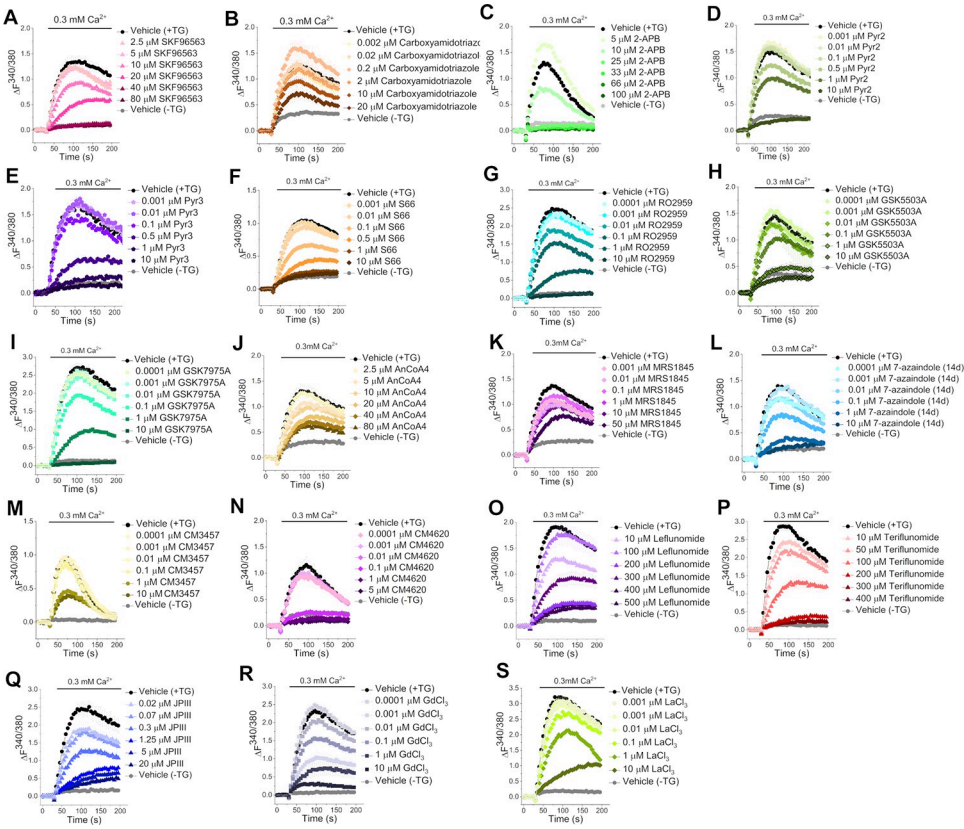

Fig 2. Example fluorescence versus time graphs for each of the inhibitors studied at the concentrations used to generate the dose response curves (Fig 3). $\Delta F^{340/380}$ refers to the ratio of fluorescence emission following excitation at 340 nm and 380 nm. Data has been baseline corrected to zero. Ca^{2+} addback is initiated at t = 30 seconds. Data points are presented as mean ± SEM (n = 3).

https://doi.org/10.1371/journal.pone.0296065.g002

for each compound (Fig 3) with a standard pre-incubation of 30 mins. All data used for subsequent IC_{50} calculations can be found in S1 Dataset.

SKF96365 (1) was originally identified as an inhibitor of receptor-mediated Ca^{2+} entry [70], and of nonselective cation currents [71]. It is better known as a TRP channel inhibitor [72,73], and it also inhibits T-type Ca^{2+} channels [74]. It reportedly inhibits SOCE with an IC_{50} of 4 μM in patch clamp studies of rat peritoneal mast cells using Fura-2 as a Ca^{2+} indicator [75]. It has also been reported to inhibit SOCE with an IC_{50} of 12 μM in Jurkat E6-1 lymphocytes, using the Indo1 dye in a fluorescence assay, which was supported by patch clamp data [76]. Under our assay conditions SKF96365 (**1**) showed almost complete block of SOCE at 40 μM, but only partial block at 10 μM (Fig 2A), which generated an IC_{50} of 16 μM (Fig 3A), roughly consistent with the previously published values observed in Jurkat T cell assays.

Carboxyamidotriazole (CAI, 2) was originally identified as a Ca^{2+} influx inhibitor. It is also a general inhibitor of non-voltage gated Ca^{2+} influx [77]. A dose-dependent reduction in Ca^{2+} influx by CAI has been reported using an assay setup similar to ours, with an IC_{50} of 0.5 μM when a 5-minute pre-incubation was used [78]. In our hands, CAI (2, used as the free amine) showed partial inhibition of SOCE in HEK293 cells at 10 μM with better inhibition at 20 μM, the highest dose tested (Fig 2B). We therefore generated an IC_{50} of 18.1 μM (Fig 3B), which was significantly higher than the published values.

2-APB (3) was originally identified as an inhibitor of inositol trisphosphate (IP_3)-modulated Ca^{2+} release [79], but it has a less straightforward effect on SOCE than other inhibitors–the

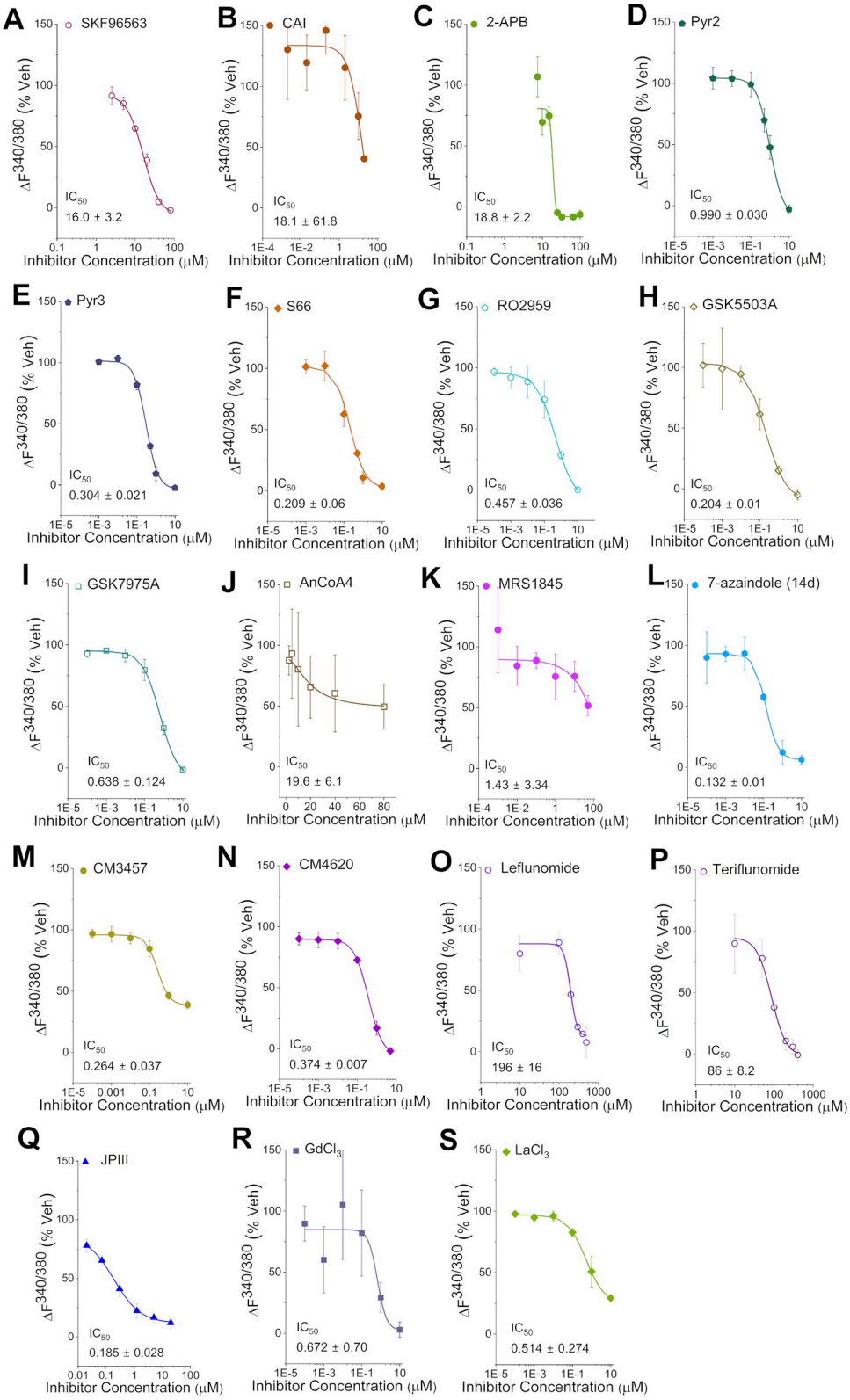

Fig 3. IC_{50} curves for SOCE inhibitory activity of the compounds profiled. Data presented as mean ± SD (n = 3). IC_{50} value derived from a fitted Hill1 equation.

https://doi.org/10.1371/journal.pone.0296065.g003

current is rapidly enhanced at low concentrations (~1–5 μM), but is inhibited at ≥10 μM in Jurkat T cells, RBL cells and DT40 B lymphocytes [80]. 2-APB was challenging to work with due to its activating effect at the lowest concentrations we tested (Fig 2C). It was difficult to record complete inactivity and therefore generating a reliable IC_{50} curve for 2-APB (3) was challenging (Fig 3C). In our hands the IC_{50} of 2-APB was calculated as ~19 μM which was three to five-fold less potent than published for CHO, HeLa and DT40 cells [81].

The 3,5-bis(trifluoromethyl)pyrazole (BTP) series were identified from a high-throughput screen to find novel IL-2 inhibitors for clinical use as immunosuppressants [82]. They are believed to block the nuclear import of nuclear factor of activated T-cells (NFAT) and thereby prevent NFAT-dependent transcription of pro-inflammatory genes. BTP2, (also known as Pyr2) was identified from this study [83]. Pyr2 was found to inhibit SOCE in Jurkat T cells with an IC_{50} of 10–100 nM, depending on the incubation time [84,85]. A different publication reported IC_{50} values of 0.59 μM for Pyr2 (4) and 0.54 μM for its sister compound, Pyr3 (5), for endogenous SOCE in RBL-2H3 cells [86]. In our hands, Pyr2 (4) showed complete inhibition of SOCE at 10 μM (Fig 2D), resulting in an IC_{50} of 990 nM (Fig 3D). Its close relative Pyr3 (5) showed very similar behaviour with slightly more potent block of SOCE at 1 μM concentration (Fig 2E), producing an IC_{50} of 304 nM (Fig 3E). Our Pyr2 (4) IC_{50} appears a little higher than the previously reported values, whilst our Pyr3 (5) IC_{50} is in agreement with published IC_{50} values recorded in RBL-2H3 cells [86].

Synta Pharmaceuticals (now Madrigal Pharmaceuticals) hold a patent on a series of SOCE inhibitors for immune and inflammatory disorders [87]. Lead compound Synta-66 (6) has been screened against a commercial panel of membrane proteins and ion channels and no significant activity was found [24]. It is a moderately potent SOCE inhibitor in blood cells, with IC_{50} values of ~1 μM in Jurkat T [24], 1.4 μM in RBL [24] and 3 μM in RBL-1 cells [88], respectively. However, it is highly potent in VSMCs and HUVECs, with an IC_{50} of ~26 nM for both [68,69] and shown to have no effect on STIM1/STIM1 clustering, TRP channels or the nonselective cationic current in VSMCs, which implies that it is not a general ion channel inhibitor [68,69] Synta-66 (6) was moderately potent showing almost complete block at 1 μM (Fig 2F). The IC_{50} of 209 nM (Fig 3F) falls well within the range of IC_{50} values obtained across a range of cell types.

Hoffmann-La Roche holds patents on SOCE inhibitors for the treatment of immune or inflammatory disorders, one of which claims their lead compound RO2959 (7) to have an IC_{50} of 15 nM for IL-2 inhibition [89]. It had an IC_{50} for SOCE inhibition of 402 nM in RBL-2H3 and 265 nM in $CD4^+$ T cells [90]. RO2959 demonstrated an IC_{50} of 25 nM for T-Rex-CHO (Chinese hamster ovary) cells overexpressing ORAI1/STIM1 vs. 530 nM in ORAI3/STIM1 overexpressing cells as measured by patch clamp [90], which represents a 20-fold selectivity ratio for ORAI1. RO2959 (7) in our hands produced complete inhibition at 10 μM (Fig 2G) producing an IC_{50} of 457 nM (Fig 3G) which are consistent with data obtained from RBL-2H3 cells and CD4+ T-cells [90].

GlaxoSmithKline (GSK) holds a patent on a series of pyrazole-based SOCE inhibitors for the treatment of allergic and immune disorders [66]. GSK5503A (8) and GSK7975A (9) were confirmed to block Ca^{2+} currents at 10 μM in patch clamp experiments in HEK293 cells [91]. GSK7975A was further characterized to demonstrate a very similar IC_{50} for ORAI1 and ORAI3 inhibition (4.1 vs 3.8 μM), but GSK5503A was not further studied [91]. This study also found them to have no effect on STIM1/STIM1 clustering or the STIM1/ORAI1 interaction, implying an extracellular binding site. This finding is supported by the reduced ability of GSK7975A to inhibit SOCE against the ORAI1 E106D pore mutant (reduced Ca^{2+} selectivity), implying that a conformational change in the glutamate selectivity filter may affect compound binding [91]. GSK7975A was screened against a small panel of ion channels and receptors

overexpressed in HEK293 cells and was found to be selective against all of them (IC_{50} > 10 μM), except for an IC_{50} of 8 μM against $Ca_V1.2$ [91]. In our hands, GSK5503A (8) was found to completely inhibit SOCE at 10 μM (Fig 2H) and generated an IC_{50} of 200 nM (Fig 3H). This appeared to be slightly more potent than the related compound GSK7975A (9) which also completely blocked SOCE at 10 μM (Fig 2I) with an IC_{50} of 638 nM (Fig 3I) which was in close agreement to previously reported findings of 0.8 μM in RBL-2H3 [91] and 0.5 μM in Jurkat cells, respectively [92].

AnCoA4 (10) was identified as an ORAI1 inhibitor using a commercial small molecule microarray, which screened against minimal functional domains–purified isolated domains of ORAI1 and STIM1 that are known to be vital for SOCE activity [93]. Using this technique, only small molecules that bind to ORAI1 or STIM1 should be identified as hits, avoiding indirect SOCE inhibitors. AnCoA4 has an IC_{50} of 880 nM in HEK293T cells calculated from an NFAT reporter gene luciferase assay [93]. AnCoA4 (10) failed to inhibit SOCE at 10 μM in our assay and only demonstrated partial inhibition when tested up to 80 μM (Fig 2J) producing an IC_{50} of 19.6 μM (Fig 3J). We tested AnCoA4 over the same concentration range with a slightly longer exposure time, by including the compound during the Fura-2 loading step, which yielded a marginal improvement to produce an IC_{50} of 12.5 μM (S18 Fig).

N-propargylnitrendipine (MRS1845) was identified in a screen of 1,4-dihydropyridines as potential SOCE inhibitors, demonstrating an IC_{50} of 1.7 μM in HL-60 cells although it was also shown to have a similar potency for inhibition of L-type calcium channels (IC_{50} = 2.1 μM) [94]. In our hands, MRS1845 gave approximately a 50% block at 50 μM, the highest dose tested (Fig 2K) with an IC_{50} of 1.43 μM (Fig 3K), although this should be interpreted with caution given the lack of a sigmoidal curve upon fitting the Hill1 equation. We noted a solubility issue at 50 μM in the aqueous solution and therefore retested the compound at a slightly lower concentration of 30μM, with a longer exposure time, by including compound during the Fura-2 loading step. This yielded a higher IC_{50} of 9.06 μM (S19 Fig) although the fit of the Hill1 equation is more accurate indicating that MRS1845 performs better with a longer exposure time.

Based on the structures of Pyr2 and Synta-66, a series of 7-azaindole SOCE inhibitors were developed as potential treatments for asthma [95]. Lead compound 7-azaindole 14d (12) is a potent SOCE inhibitor with an IC_{50} of 150 nM in Jurkat T cells, showing dose-dependent inhibition of eosinophils in a rat model of allergic respiratory inflammation [95]. In our hands 7-azaindole 14d (12) showed strong, but not complete inhibition at 10 μM, (Fig 2L). The IC_{50} was calculated as 132 nM (Fig 3L) which was almost in complete agreement with the IC_{50} generated with Jurkat cells in a similar assay set-up [95].

CalciMedica holds several patents on CRAC inhibitors. Their lead compound CM4620 (14) [96], has reportedly completed Phase II clinical trials for treatment of acute pancreatitis with systemic inflammatory response syndrome (SIRS), and others are ongoing [53,97–99]. A related compound, CM3457 (13), has shown immunomodulatory effects in different cell lines, including interleukin inhibition [100] and was shown to be selective for ORAI1 inhibition over several other K^+, Na^+ and Ca^{2+} channels [100]. CM4620 (14) has an IC_{50} of ~0.1 μM in ORAI1/STIM1 overexpressing HEK293 cells, measured by whole-cell patch clamp experiments, as well as ~0.7 μM in murine pancreatic acinar cells [101]. The related compound, CM3457 (13), potently inhibits endogenous SOCE in RBL-2H3 cells with an IC_{50} of 25 nM and Jurkat T-cells with an IC_{50} of 17 nM, which were comparable to the IC_{50} of 34nM observed for HEK293 cells stably overexpressing ORAI1/STIM1 [100]. Of the CalciMedica inhibitors, CM4620 (14) showed almost complete inhibition of SOCE at 10 μM (Fig 2N) generating an IC_{50} of 374 nM (Fig 3N). This is in good agreement with a previously observed IC_{50} of ~0.1 μM in ORAI1/STIM1 overexpressing HEK293 cells [101]. The older compound

CM3457 (13) failed to show complete SOCE inhibition at 10 μM (Fig 2M) and therefore the calculated IC_{50} of 264 nM may be an overestimate of its potency (Fig 3M).

Several FDA-approved drugs have been identified as weak to moderately potent SOCE/ORAI1 inhibitors in a single study, using a ligand-based virtual screen [102]. Five drugs (leflunomide, teriflunomide, tolvaptan, lansoprazole and roflumilast) showed substantial (≥60%) SOCE inhibition at 10 μM, and a dose-response curve was generated. Leflunomide (15) and its active metabolite teriflunomide (16) showed SOCE inhibition at clinically relevant concentrations, with IC_{50} values of ~10 μM (leflunomide) and ~21 μM (teriflunomide), respectively [102], which is lower than most other reported inhibitors. Leflunomide is approved as a dihydro-orotate dehydrogenase inhibitor used to treat rheumatoid arthritis and psoriatic arthritis [103]; teriflunomide was later approved for the treatment of multiple sclerosis [104]. Under our conditions leflunomide (15) and teriflunomide (16) showed no inhibition at 10 μM, so the compounds were tested up to 500 μM and 400 μM, respectively. Partial SOCE inhibition was observed with 400 and 500 μM leflunomide (15) (Fig 2O) generating an IC_{50} of 196 μM (Fig 3O). Teriflunomide (16) was more potent providing more of a dose-response with strong inhibition above 200 μM (Fig 2P) generating an IC_{50} of 86 μM (Fig 3P), a value significantly less potent than previously quoted IC_{50} values.

Based on the structure of Synta-66, JPIII (17) was recently developed in-house as a more water-soluble alternative [31]. It is moderately potent and highly selective for ORAI1 over other Ca^{2+}-permeable channels and was well-tolerated and effective in a mouse model of cardiac hypertrophy [31] and rat model of pulmonary hypertension [105]. Overexpression of ORAI1 did not affect the potency of JPIII, only the amplitude of the fluorescence signal due to increased $[Ca^{2+}]$ [31]. JPIII (17) demonstrated partial SOCE inhibition in a dose-response manner (Fig 2Q) with an IC_{50} of 185 nM (Fig 3Q), similar to the IC_{50} of 399 nM previously reported in HEK293 cells [31].

The trivalent lanthanide cations, such as gadolinium (Gd^{3+}) (18) and lanthanum (La^{3+}) (19) are known to block SOCE in the low micromolar range, with 1 μM Gd^{3+} causing complete channel block in a range of cell lines [106–108]. Gd^{3+} inhibits SOCE with an IC_{50} of 34 nM in the rat smooth muscle A7r5 cell line [107]. La^{3+} has been found to potently inhibit SOCE in Jurkat T cells stimulated with either thapsigargin or CD3 monoclonal antibody with an IC_{50} of 20 nM [106]. Gd^{3+} (18) showed moderate inhibition of SOCE at 10 μM (Fig 2R), whilst La^{3+} (19) demonstrated partial inhibition of SOCE at 10 μM (Fig 2S). These generated IC_{50} values of 0.67 μM (Fig 3R) and ~0.5 μM (Fig 3S), respectively, which were around 20-fold less potent than reported in the literature.

To allow a cross-wise comparison of the potency of the compounds we calculated the SOCE inhibitory activity as % vehicle of each inhibitor at 10 μM in Fig 4. With the exception of CAI (2), 2-APB (3), AnCoA4 (10), MRS1845 (11), leflunomide (15) and teriflunomide (16) all tested compounds showed significant SOCE inhibitory activity at this concentration. For ease of reference our calculated IC_{50} values are shown alongside comparable values obtained from the literature in Table 1.

Discussion

A variety of reported SOCE inhibitors were tested in a standard HEK293 cell Ca^{2+} addback assay with Fura-2 as the indicator dye and thapsigargin to deplete stores. Native HEK293 cells were chosen as a model system to study SOCE, as the Ca^{2+} addback response following TG depletion has been demonstrated to be highly specific to ORAI1 [64]. Knockout of ORAI1, either alone or in combination with ORAI2 or 3 knockout completely ablated Ca^{2+} entry whilst knockout of either ORAI2, ORAI3 or double knockout of ORAI2/3 had no effect on

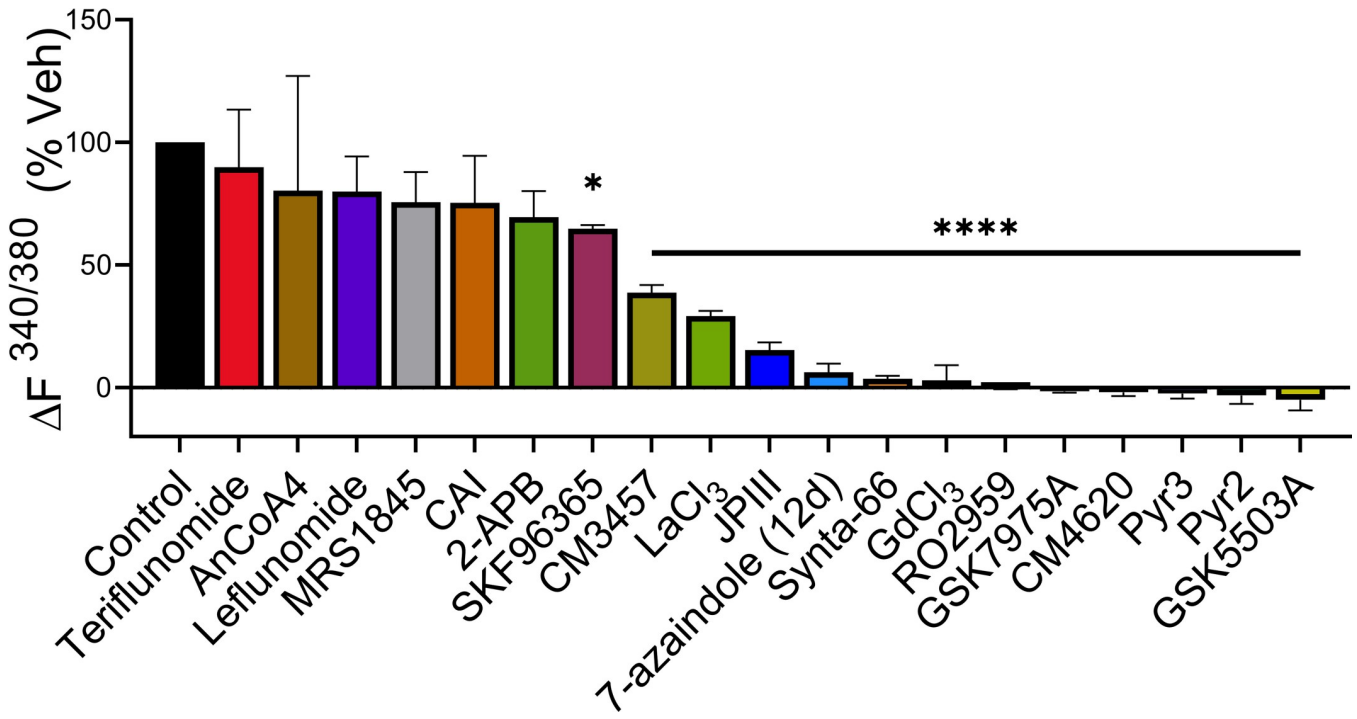

Fig 4. A comparison of the SOCE inhibitory activity as % vehicle of each inhibitor at 10 μM in the Ca^{2+} addback assay. Statistical significance was calculated using an ANOVA one-way test with Dunnett's post-hoc test, where *p<0.05, and ****p<0.0001 (n = 3).

https://doi.org/10.1371/journal.pone.0296065.g004

Ca^{2+} entry in a similar assay [64] Interestingly, overexpression of ORAI2 in ORAI1/2/3 triple knockout cells lead to a greater influx of Ca^{2+} compared to native cells, which the authors reasoned was due to the much lower expression of ORAI2 and ORAI3 compared to ORAI1 in native HEK293 cells [64]. Differing IC_{50} values have been reported for compounds between native HEK293 cells and those overexpressing ORAI1 and/or STIM1 [93]. These studies highlight the caution needed when extrapolating data from overexpression systems to the native *in vivo* environment. Under our assay conditions most compounds showed significant SOCE inhibition. We were able to demonstrate that the most potent inhibitors in this side-by-side comparison were: 7-azaindole 14d (12), JPIII (17), Synta-66 (6), Pyr 3 (5), GSK5503A (8), CM4620 (14) and RO2959 (7)—all giving IC_{50} values < 0.5μM. Of the compounds tested: SKF96365 (1), Pyr3 (5), Synta-66 (6), RO2959 (7), GSK7975A (9), MRS1845 (11), 7-azaindole 14d (12), CM4620 (14), and JPIII (17) generated IC_{50} values consistent with the literature. Conversely, CAI (2), 2-APB (3), Pyr2 (4), AnCoA4 (10), CM3457 (13), Leflunomide (15), Teriflunomide (16), Gd^{3+} (18) and La^{3+} (19) generated IC_{50} values greater than published values.

In our assay, CAI (2) did not demonstrate full inhibition of SOCE at 20 μM, the highest dose tested. This was surprising given that a one hour pretreatment with 5 μM CAI inhibited SOCE in three different ovarian cancer cell lines using a similar assay setup [109] and in another study an IC_{50} of 0.5 μM was generated when a 5-minute pre-incubation was used [78]. The authors noted inhibition to be time-dependent, with 40% inhibition seen at 10 μM after a 10-second pre-incubation with CAI, compared with complete block after 5 minutes [78]. The time-dependence was also confirmed by whole-cell patch clamp experiments, and it was suggested to act via a complex mechanism affecting mitochondrial membrane polarisation rather than as a simple ion channel blocker [78]. In our assay setup cells were pre-incubated with test compound for 30 minutes, which should be sufficient to observe an effect for CAI based on the literature.

Table 1. SOCE inhibitory activity (IC_{50} ± SE) of the SOCE inhibitors studied, compared to their reported IC_{50} values.

Compound name	Residual Ca^{2+} entry at 10μM	IC_{50} (HEK293) / μM ± SE	Reported SOCE inhibition IC_{50} / μM	Cell line for reported IC_{50}
SKF96365 (**1**)	64.9%	16.0 ± 1.8	4 12	rat peritoneal mast cells [75] Jurkat E6-1 lymphocytes [76]
CAI (**2**)	75.4%	18.1 ± 61.8	0.5	HEK293 [78]
2-APB (**3**)	69.5%	18.8 ± 2.2	2.9 ± 0.1 4.8 ± 0.6 6.5 ± 0.3	CHO [81] IP_3R-knockout DT40 [81] HeLa [81]
Pyr2 (**4**)	0%	0.990 ± 0.030	0.01–0.1 0.59	Jurkat T cells [84, 85] RBL-2H3 [86]
Pyr3 (**5**)	0%	0.304 ± 0.021	0.54	RBL-2H3 [86]
Synta-66 (**6**)	3.6%	0.209 ± 0.06	0.026 0.026 1.4 ~1 3	VSMC [68,69] HUVEC [68,69] RBL [24] Jurkat T cells [24] RBL-1 [88]
RO2959 (**7**)	0%	0.457 ± 0.036	0.265 ± 0.016 0.402 ± 0.129	human $CD4^+$ T-cells [90] RBL-2H3 [90]
GSK5503A (**8**)	0%	0.204 ± 0.01	Full block at 10 μM	HEK-293 overexpressing ORAI1/STIM1 [91]
GSK7975A (**9**)	0%	0.638 ± 0.124	0.5 0.8 ± 0.1	human $CD4^+$ T-cells [92] RBL-2H3 [91]
AnCoA4 (**10**)	95.8%	19.6 ± 6.1	0.88	IC_{50} in HEK293T, NFAT inhibition [93]
MRS1845 (**11**)	75.7%	1.43 ±??	1.7	HL60 cells [94]
7-azaindole (**12**)	6.2%	0.132 ± 0.01	0.150 ± 0.022	Jurkat T cells [95]
CM3457 (**13**)	38.8%	0.264 ± 0.037	0.017 0.025 0.034	Jurkat T cells [100] RBL-2H3 [100] HEK293 overexpressing ORAI1/STIM1 [100]
CM4620 (**14**)	0%	0.374 ± 0.007	0.1 0.7	HEK293 overexpressing ORAI1/STIM1 [101] human pancreatic acinar cells [101]
Leflunomide (**15**)	80%	196 ± 16	~10	RBL-1 [102]
Teriflunomide (**16**)	90%	86 ± 8.2	~21	RBL-1 [102]
JPIII (**17**)	15.3%	0.185 ± 0.028	0.399	HEK293 [31]
Gd^{3+} (**18**)	2.96%	0.672 ± 0.70	0.034 ± 0.005	A7r5 [107]
La^{3+} (**19**)	28.5%	0.514 ± 0.274	0.02	Jurkat T cells [106]

Reported inhibition refers to endogenous SOCE unless stated. Literature inhibition values only include those from similar cell-based Ca^{2+} addback assays, with standard error reported where given. All IC_{50} values were generated in native HEK293 cells (n = 3).

https://doi.org/10.1371/journal.pone.0296065.t001

2-APB (3), proved technically challenging to work with due to its well established activating effect at the lowest concentrations tested and inhibitory effect at higher concentrations [80]. Given these difficulties the IC_{50} we recorded was -three to -fivefold less potent than published values. The effects of 2-APB are variable between ORAI1/ORAI2/ORAI3 [110]. 2-APB can interact with other ion channels and receptors that influence SOCE, including TRP channels, the IP_3 receptor and the SERCA pump [111], alongside ORAI2 and ORAI3 [112].

Pyr2 (4) was initially described as the first selective CRAC channel inhibitor [83,85] but was later found to inhibit TRPC3 and TRPC5 channels, and to activate TRPM4 [113,114]. It has been proposed to inhibit from the extracellular space based on patch clamp experiments [85].

Our IC_{50} value of ~1 μM was higher than the range of values reported (10–590 nM) [84–86,90], possibly due to the difference in incubation time. In one study the cells were incubated in test compound for a few minutes [84], whereas in another study they were incubated for 24 hours, with maximal block seen after 2 hours [85].

AnCoA4 (10) had a reported IC_{50} of 880 nM (HEK293T), as measured using an NFAT reporter gene luciferase assay, which is an indirect measure of SOCE using a downstream signalling pathway [93]. It has been validated as a SOCE inhibitor by other groups [115–117], and also showed 80% inhibition of Ca^{2+} current (20 μM) in patch clamp studies of ORAI1 [93], but a dose-response for direct inhibition of SOCE was not determined in any of these studies. AnCoA4 was proposed to act intracellularly by blocking the ORAI1/STIM1 interaction [93], Repurchased AnCoA4 failed to completely inhibit SOCE in our assay at 80 μM, the highest dose tested. In the NFAT luciferase assay, the cells were pre-incubated with AnCoA4 for 6 hours before initiation of SOCE, whereas our assay only has a 30-minute compound incubation step. We tested AnCoA4 with a longer pre-incubation by adding AnCoA4 during the Fura-2 loading step such that cells were exposed to the compound for 90 mins in total. We observed a modest improvement in IC_{50} with the longer pre-incubation, but still did not achieve complete SOCE inhibition at the highest dose.

MRS1845 (11) was previously shown to have an IC_{50} of 1.7 μM in HL-60 cells [94], but ATP was used as the stimulus for SOCE instead of thapsigargin. In our hands, MRS1845 achieved approximately a 50% block of SOCE at 50μM with little to no block at 10 μM, although we noted solubility issues at the higher concentrations in aqueous solution. Our results are in agreement with a lack of potency observed against convulxin/thrombin stimulated SOCE in platelets at concentrations up to 100 μM [118]. Others have reported potency of MRS1845 against thapsigargin-induced SOCE in a Fura-2 based assay in both ovarian carcinoma cells [119] and human aortic smooth muscle cells [120,121] although exposure to MRS1845 was for 24 hours indicating it may act on SOCE in an indirect manner.

In our hands, CM3457 (13) failed to completely inhibit SOCE at the highest concentration tested (10μM) and was around 10-fold less potent in native HEK293 cells than observed in a Fluo-4 based assay of ORAI1 overexpressing HEK293 cells or immune cells [100]. Due to the low amplitude of the I_{CRAC} current, overexpressing cells are often used to increase the amplitude of the addback response by fluorescence imaging for ease of measurement and this could account for the observed difference. The FDA-approved drugs although still active in our assay were significantly less potent–leflunomide (16) by ~10-fold and teriflunomide (17) by ~4-fold. This is a large discrepancy when the only major difference is the cell line (RBL-1), -assay, pre-incubation times, dye and the mode of store depletion were similar [122].

The trivalent lanthanide cation Gd^{3+} (18) inhibits SOCE with an IC_{50} of 34 nM in the rat smooth muscle A7r5 cell line [107]. This study used a similar assay setup, with thapsigargin and Fura-2, although the imaging technique and cell line differed [107]. It also inhibited with a similar potency (IC_{50} = 50 nM) in patch clamp studies in the Drosophila S2 cell line [123]. La^{3+} (19) has been found to potently inhibit SOCE in Jurkat T cells stimulated with either thapsigargin or CD3 monoclonal antibody with an IC_{50} of 20 nM [106]. This assay used a fluorescence-activated cell sorter (FACS)-based measurement system with Indo-1 as the indicator dye, which could account for the observed difference in potency. Both Gd^{3+} and La^{3+} are less potent than the literature value in our hands, by around 20-fold, but both still retain their characteristic sub-micromolar potency. Lanthanides are not cell-permeable, and so are believed to act by simply blocking the pore [106]. However, they may act at a different binding site to Ca^{2+}, as no change in La^{3+} block is seen for the well-established E106D pore mutant, which is characterised by a loss of Ca^{2+} selectivity [124]. Whilst lanthanides are widely used to study

channel blockade *in vitro*, they would not be useful therapeutically as they block a variety of cation channels, and various toxic effects have been observed [125].

Although approximately half of the compounds tested were confirmed to display similar potencies to those recorded in the literature there were discrepancies in potency observed for the remaining compounds. This could be due to differences in assay setup, choice of fluorescent dye, equipment used to quantify [Ca^{2+}], or differences in SOCE pathways in different cell lines. As compound binding to ORAI1 has not been empirically proven for most inhibitors, it is possible that some act upstream of the SOCE pathway rather than directly targeting it. This could also be the reason some compounds require longer pre-incubation periods and so did not appear to be active in this assay. This highlights the difficulty in developing a 'one-size-fits-all' assay, as a short pre-incubation step may lead to compounds with a slower mechanism of action being missed during screenings, but longer pre-incubations may not be feasible for a cell-based assay as extended Ca^{2+} depletion is cytotoxic.

The choice of cell line is likely to be an important reason for variability in potency data. Studies using RBL cells for SOCE assays are often inconsistent with the results acquired here in HEK293 cells. Synta-66 (6) is much less potent in RBL-1 cells than in HEK293 cells (3 μM vs. 130 nM). In the related line RBL-2H3, Pyr3 (5), RO2959 (7) and GSK7975A (9) show comparable potency to that observed in HEK293 cells, although CM3457 (13) is around 10-fold less potent (0.264 vs. 0.025 nM). Native RBL-2H3 cells express higher levels of ORAI1 and ORAI2 than HEK293 and they thus demonstrate a larger SOCE amplitude [126]. There may also be differences between species–HEK293, Jurkat T, HeLa and $CD4^+$ cells are human cell lines, while RBL cells are from rats, CHO cells from hamsters and DT40 cells from chickens. GSK7975A (9) and its analogue GSK5498A have been previously observed to have species-dependent effects. They inhibit production of mast cell mediators and pro-inflammatory T cell cytokines in human and rat mast cells, but not in mouse or guinea pig [92]. Differences in potency of compounds may be observed between native and ORAI1-overexpressing cells, the latter being of particular use in patch clamp experiments, where the native ORAI1 current can be difficult to isolate, an issue that is not apparent when recordings are obtained from a confluent layer of cells, as occurs when using the FlexStation. Patch clamp is widely used to study ion channel inhibitor binding and was used to validate many of the profiled compounds in the literature. However, patch clamp is technically challenging and so time-consuming it is unsuitable for routine screening on drug discovery projects, although high-throughput automated patch clamp technologies have become available [127]. Although no assay is perfect the Fura-2 based assay of thapsigargin induced store depletion is well established as a reliable method of monitoring SOCE and when performed on the FlexStation III it can be used as a high-throughput screening tool. Limitations of the current study include that the TG-induced store depletion phase fell outside of the recording window as to record it would have necessitated significantly lengthening the recording window, with concomitant lengthy exposure to Ca^{2+}-free conditions having an adverse effect on cell viability. Additionally, we have made the assumption that the SOCE signal was derived from activity of ORAI1 given recent reports that confirm knock-out of ORAI1 in HEK293 largely abolishes the TG-induced SOCE signal [64,65]. However, it is beyond the scope of this study to characterize all of the Ca^{2+} selective channels that could have been affected by each of the compounds.

Nonetheless, inhibitors of SOCE represent a valuable class of compounds as potential therapeutics in a variety of disease areas, including immunoinflammatory disease, cardiovascular disease and cancer. This study highlights the importance of assay design and use of biorthogonal assays to validate a novel compound. These data also provide a fair comparison of most SOCE inhibitors in a standard and well-validated assay, and so may aid others in choosing the most suitable molecule for a specific application.

Supporting information

S1 Fig. Chemical structures of the small molecule SOCE inhibitors examined in this study and their common names.
(TIF)

S2 Fig. Convergent synthetic route to GSK7975A (9).
(TIF)

S3 Fig. Synthesis of GSK5503A (8) from intermediate 21.
(TIF)

S4 Fig. Synthetic route to 7-azaindole (12).
(TIF)

S5 Fig. ^{1}H NMR (400 MHz, DMSO-D_6) (top) and ^{13}C NMR (100 MHz, DMSO-D_6) (bottom) spectra of 2,6-difluoro-*N*-(1*H*-pyrazol-3-yl)benzamide (21).
(TIF)

S6 Fig. ^{1}H NMR (500 MHz, methanol-D_4) (top) and ^{13}C NMR (100 MHz, methanol-D_4) (bottom) spectra of 3-trifluoromethyl-4-(hydroxymethyl)phenol (18).
(TIF)

S7 Fig. ^{1}H NMR (400 MHz, $CDCl_3$) (top) and ^{13}C NMR (100 MHz, $CDCl_3$) (bottom) spectra of [4-(benzyloxy)-2-(trifluoromethyl)phenyl]methanol (19).
(TIF)

S8 Fig. ^{1}H NMR (500 MHz, $CDCl_3$) (top) and ^{13}C NMR (100 MHz, $CDCl_3$) (bottom) spectra of N-(1-{[4-(benzyloxy)-2-(trifluoromethyl)phenyl]methyl)-1H-pyrazol-3-yl)-2,6-difluorobenzamide (22).
(TIF)

S9 Fig. ^{1}H NMR (500 MHz, methanol-D_4) (top) and ^{13}C NMR (100 MHz, methanol-D_4) (bottom) spectra of 2,6-difluoro-N-(1-{[4-hydroxy-2-(trifluoromethyl)phenyl]methyl}-1H-pyrazol-3-yl)benzamide (9).
(TIF)

S10 Fig. ^{1}H NMR (500 MHz, methanol-D_4) (top) and ^{13}C NMR (125 MHz, methanol-D_4) (bottom) spectra of 2,6-difluoro-*N*-{1-[(2-phenoxyphenyl)methyl]-1*H*-pyrazol-3-yl}benzamide (8).
(TIF)

S11 Fig. ^{1}H NMR (400 MHz, $CDCl_3$) (top) and ^{13}C NMR (100 MHz, $CDCl_3$) (bottom) spectra of [(2-chloro-6-fluorophenyl)ethynyl](trimethyl)silane (25).
(TIF)

S12 Fig. ^{1}H NMR (400 MHz, $CDCl_3$) (top) and ^{13}C NMR (100 MHz, $CDCl_3$) (bottom) spectra of 1-chloro-2-ethynyl-3-fluorobenzene (26).
(TIF)

S13 Fig. ^{1}H NMR (400 MHz, DMSO-D_6) (top) and ^{13}C NMR (100 MHz, DMSO-D_6) (bottom) spectra of 5-bromo-3-[(2-chloro-6-fluorophenyl)ethynyl]pyridin-2-amine (27).
(TIF)

S14 Fig. ^{1}H NMR (400 MHz, $CDCl_3$) (top) and ^{13}C NMR (100 MHz, $CDCl_3$) (bottom) spectra of 5-bromo-2-(2-chloro-6-fluorophenyl)-1H-pyrrolo[2,3-b]pyridine (28).
(TIF)

S15 Fig. ^{1}H NMR (400 MHz, $CDCl_3$) (top) and ^{13}C NMR (100 MHz, $CDCl_3$) (bottom) spectra of 5-bromo-2,4-dimethoxypyridine (29).
(TIF)

S16 Fig. ^{1}H NMR (400 MHz, $CDCl_3$) (top) and ^{13}C NMR (100 MHz, $CDCl_3$) (bottom) spectra of 4,6-dimethoxypyridin-3-yl)boronic acid (30).
(TIF)

S17 Fig. ^{1}H NMR (400 MHz, $CDCl_3$) (top) and ^{13}C NMR (100 MHz, $CDCl_3$) (bottom) spectra of 2-(2-chloro-6-fluorophenyl)-5-(4,6-dimethoxypyridin-3-yl)-1H-pyrrolo[2,3-b]pyridine (12).
(TIF)

S18 Fig. Example fluorescence over time graph (A) and IC_{50} (B) for AnCoA4 following 30 minute preincubation and example fluorescence over time graph (C) and IC_{50} (D) for AnCoA4 following 90 minute preincubation.
(TIF)

S19 Fig. Example fluorescence over time graph (A) and IC_{50} (B) for MRS1845 following 30 minute preincubation and example fluorescence over time graph (C) and IC_{50} (D) for MRS1845 following 90 minute preincubation.
(TIF)

S1 Appendix. Detailed methods for compound synthesis.
(PDF)

S1 Dataset. Raw data used to calculate IC_{50} values. Baseline corrected $\Delta^{340/380}$ ratios from three independent biological replicates (Plate A, B and C) which each included three technical replicates for each condition tested.
(XLSX)

Author Contributions

Conceptualization: Marc A. Bailey.

Formal analysis: Katherine Norman, Karen E. Hemmings, Heba Shawer, Hollie L. Appleby, Alan J. Burnett, Nurasyikin Hamzah, Rajendra Gosain, Emily M. Woodhouse.

Funding acquisition: David J. Beech, Richard Foster, Marc A. Bailey.

Investigation: Katherine Norman, Karen E. Hemmings, Heba Shawer, Hollie L. Appleby, Alan J. Burnett, Nurasyikin Hamzah, Rajendra Gosain, Emily M. Woodhouse.

Methodology: Katherine Norman.

Project administration: David J. Beech, Richard Foster, Marc A. Bailey.

Resources: David J. Beech, Richard Foster.

Supervision: David J. Beech, Richard Foster, Marc A. Bailey.

Validation: Katherine Norman.

Visualization: Katherine Norman, Karen E. Hemmings, Heba Shawer.

Writing – original draft: Katherine Norman.

Writing – review & editing: Katherine Norman, Karen E. Hemmings, Heba Shawer, Hollie L. Appleby, Alan J. Burnett, Nurasyikin Hamzah, Rajendra Gosain, Emily M. Woodhouse, David J. Beech, Richard Foster, Marc A. Bailey.

References

1. Clapham DE. Calcium signaling. Cell. 2007; 131(6):1047–58. https://doi.org/10.1016/j.cell.2007.11.028 PMID: 18083096
2. Putney JW Jr. A model for receptor-regulated calcium entry. Cell Calcium. 1986; 7(1):1–12. https://doi.org/10.1016/0143-4160(86)90026-6 PMID: 2420465
3. Parekh AB, Penner R. Store depletion and calcium influx. Physiol Rev. 1997; 77(4):901–30. https://doi.org/10.1152/physrev.1997.77.4.901 PMID: 9354808
4. Feske S, Gwack Y, Prakriya M, Srikanth S, Puppel SH, Tanasa B, et al. A mutation in Orai1 causes immune deficiency by abrogating CRAC channel function. Nature. 2006; 441(7090):179–85. https://doi.org/10.1038/nature04702 PMID: 16582901
5. Vig M, Peinelt C, Beck A, Koomoa DL, Rabah D, Koblan-Huberson M, et al. CRACM1 is a plasma membrane protein essential for store-operated Ca2+ entry. Science. 2006; 312(5777):1220–3. https://doi.org/10.1126/science.1127883 PMID: 16645049
6. Zhang SL, Yeromin AV, Zhang XH, Yu Y, Safrina O, Penna A, et al. Genome-wide RNAi screen of Ca(2+) influx identifies genes that regulate Ca(2+) release-activated Ca(2+) channel activity. Proc Natl Acad Sci U S A. 2006; 103(24):9357–62. https://doi.org/10.1073/pnas.0603161103 PMID: 16751269
7. Potier M, Gonzalez JC, Motiani RK, Abdullaev IF, Bisaillon JM, Singer HA, et al. Evidence for STIM1- and Orai1-dependent store-operated calcium influx through ICRAC in vascular smooth muscle cells: role in proliferation and migration. Faseb j. 2009; 23(8):2425–37. https://doi.org/10.1096/fj.09-131128 PMID: 19364762
8. Liou J, Kim ML, Heo WD, Jones JT, Myers JW, Ferrell JE Jr., et al. STIM is a Ca2+ sensor essential for Ca2+-store-depletion-triggered Ca2+ influx. Curr Biol. 2005; 15(13):1235–41. https://doi.org/10.1016/j.cub.2005.05.055 PMID: 16005298
9. Park CY, Hoover PJ, Mullins FM, Bachhawat P, Covington ED, Raunser S, et al. STIM1 clusters and activates CRAC channels via direct binding of a cytosolic domain to Orai1. Cell. 2009; 136(5):876–90. https://doi.org/10.1016/j.cell.2009.02.014 PMID: 19249086
10. Hou X, Pedi L, Diver MM, Long SB. Crystal structure of the calcium release-activated calcium channel Orai. Science. 2012; 338(6112):1308–13. https://doi.org/10.1126/science.1228757 PMID: 23180775
11. Cai X, Zhou Y, Nwokonko RM, Loktionova NA, Wang X, Xin P, et al. The Orai1 Store-operated Calcium Channel Functions as a Hexamer. J Biol Chem. 2016; 291(50):25764–75. https://doi.org/10.1074/jbc.M116.758813 PMID: 27780862
12. Hou X, Outhwaite IR, Pedi L, Long SB. Cryo-EM structure of the calcium release-activated calcium channel Orai in an open conformation. Elife. 2020; 9. https://doi.org/10.7554/eLife.62772 PMID: 33252040
13. Liu X, Wu G, Yu Y, Chen X, Ji R, Lu J, et al. Molecular understanding of calcium permeation through the open Orai channel. PLoS Biol. 2019; 17(4):e3000096. https://doi.org/10.1371/journal.pbio.3000096 PMID: 31009446
14. Derler I, Fahrner M, Carugo O, Muik M, Bergsmann J, Schindl R, et al. Increased hydrophobicity at the N terminus/membrane interface impairs gating of the severe combined immunodeficiency-related ORAI1 mutant. J Biol Chem. 2009; 284(23):15903–15. https://doi.org/10.1074/jbc.M808312200 PMID: 19366689
15. Maus M, Jairaman A, Stathopulos PB, Muik M, Fahrner M, Weidinger C, et al. Missense mutation in immunodeficient patients shows the multifunctional roles of coiled-coil domain 3 (CC3) in STIM1 activation. Proc Natl Acad Sci U S A. 2015; 112(19):6206–11. https://doi.org/10.1073/pnas.1418852112 PMID: 25918394
16. Yu F, Agrebi N, Mackeh R, Abouhazima K, KhudaBakhsh K, Adeli M, et al. Novel ORAI1 Mutation Disrupts Channel Trafficking Resulting in Combined Immunodeficiency. J Clin Immunol. 2021; 41(5):1004–15. https://doi.org/10.1007/s10875-021-01004-8 PMID: 33650027
17. Kaufmann U, Shaw PJ, Kozhaya L, Subramanian R, Gaida K, Unutmaz D, et al. Selective ORAI1 Inhibition Ameliorates Autoimmune Central Nervous System Inflammation by Suppressing Effector but Not Regulatory T Cell Function. J Immunol. 2016; 196(2):573–85. https://doi.org/10.4049/jimmunol.1501406 PMID: 26673135

18. Kim JH, Carreras-Sureda A, Didier M, Henry C, Frieden M, Demaurex N. The TAM-associated STIM1 (I484R) mutation increases ORAI1 channel function due to a reduced STIM1 inactivation break and an absence of microtubule trapping. Cell Calcium. 2022; 105:102615. https://doi.org/10.1016/j.ceca.2022.102615 PMID: 35792400

19. Nesin V, Wiley G, Kousi M, Ong EC, Lehmann T, Nicholl DJ, et al. Activating mutations in STIM1 and ORAI1 cause overlapping syndromes of tubular myopathy and congenital miosis. Proc Natl Acad Sci U S A. 2014; 111(11):4197–202. https://doi.org/10.1073/pnas.1312520111 PMID: 24591628

20. Eckstein M, Lacruz RS. CRAC channels in dental enamel cells. Cell Calcium. 2018; 75:14–20. https://doi.org/10.1016/j.ceca.2018.07.012 PMID: 30114531

21. Markello T, Chen D, Kwan JY, Horkayne-Szakaly I, Morrison A, Simakova O, et al. York platelet syndrome is a CRAC channelopathy due to gain-of-function mutations in STIM1. Mol Genet Metab. 2015; 114(3):474–82. https://doi.org/10.1016/j.ymgme.2014.12.307 PMID: 25577287

22. Böhm J, Bulla M, Urquhart JE, Malfatti E, Williams SG, O'Sullivan J, et al. ORAI1 Mutations with Distinct Channel Gating Defects in Tubular Aggregate Myopathy. Hum Mutat. 2017; 38(4):426–38. https://doi.org/10.1002/humu.23172 PMID: 28058752

23. Clemens RA, Lowell CA. CRAC channel regulation of innate immune cells in health and disease. Cell Calcium. 2019; 78:56–65. https://doi.org/10.1016/j.ceca.2019.01.003 PMID: 30641250

24. Di Sabatino A, Rovedatti L, Kaur R, Spencer JP, Brown JT, Morisset VD, et al. Targeting gut T cell Ca2+ release-activated Ca2+ channels inhibits T cell cytokine production and T-box transcription factor T-bet in inflammatory bowel disease. J Immunol. 2009; 183(5):3454–62. https://doi.org/10.4049/jimmunol.0802887 PMID: 19648266

25. Lee C, Xu D-Z, Feketeova E, Kannan KB, Deitch EA, Livingston DH, et al. Store-operated calcium channel inhibition attenuates neutrophil function and post-shock acute lung injury. Journal of the American College of Surgeons. 2004; 199(3, Supplement):36–7. https://doi.org/10.197/01.ta.0000171456.54921.fe

26. Waldron RT, Chen Y, Pham H, Go A, Su HY, Hu C, et al. The Orai Ca(2+) channel inhibitor CM4620 targets both parenchymal and immune cells to reduce inflammation in experimental acute pancreatitis. J Physiol. 2019; 597(12):3085–105. https://doi.org/10.1113/JP277856 PMID: 31050811

27. Johnson M, Trebak M. ORAI channels in cellular remodeling of cardiorespiratory disease. Cell Calcium. 2019; 79:1–10. https://doi.org/10.1016/j.ceca.2019.01.005 PMID: 30772685

28. Luo R, Gomez AM, Benitah JP, Sabourin J. Targeting Orai1-Mediated Store-Operated Ca(2+) Entry in Heart Failure. Front Cell Dev Biol. 2020; 8:586109. https://doi.org/10.3389/fcell.2020.586109 PMID: 33117812

29. Mohis M, Edwards S, Ryan S, Rizvi F, Tajik AJ, Jahangir A, et al. Aging-related increase in store-operated Ca(2+) influx in human ventricular fibroblasts. Am J Physiol Heart Circ Physiol. 2018; 315(1):H83–h91. https://doi.org/10.1152/ajpheart.00588.2017 PMID: 29985070

30. Rosenberg P, Katz D, Bryson V. SOCE and STIM1 signaling in the heart: Timing and location matter. Cell Calcium. 2019; 77:20–8. https://doi.org/10.1016/j.ceca.2018.11.008 PMID: 30508734

31. Bartoli F, Bailey MA, Rode B, Mateo P, Antigny F, Bedouet K, et al. Orai1 Channel Inhibition Preserves Left Ventricular Systolic Function and Normal Ca(2+) Handling After Pressure Overload. Circulation. 2020; 141(3):199–216. https://doi.org/10.1161/CIRCULATIONAHA.118.038891 PMID: 31906693

32. Wang J, Xu C, Zheng Q, Yang K, Lai N, Wang T, et al. Orai1, 2, 3 and STIM1 promote store-operated calcium entry in pulmonary arterial smooth muscle cells. Cell Death Discov. 2017; 3:17074. https://doi.org/10.1038/cddiscovery.2017.74 PMID: 29188077

33. Van Assche T, Fransen P, Guns PJ, Herman AG, Bult H. Altered Ca2+ handling of smooth muscle cells in aorta of apolipoprotein E-deficient mice before development of atherosclerotic lesions. Cell Calcium. 2007; 41(3):295–302. https://doi.org/10.1016/j.ceca.2006.06.010 PMID: 16999997

34. Liang SJ, Zeng DY, Mai XY, Shang JY, Wu QQ, Yuan JN, et al. Inhibition of Orai1 Store-Operated Calcium Channel Prevents Foam Cell Formation and Atherosclerosis. Arterioscler Thromb Vasc Biol. 2016; 36(4):618–28. https://doi.org/10.1161/ATVBAHA.116.307344 PMID: 26916730

35. Beech DJ. Orai1 calcium channels in the vasculature. Pflugers Arch. 2012; 463(5):635–47. https://doi.org/10.1007/s00424-012-1090-2 PMID: 22402985

36. Shawer H, Norman K, Cheng CW, Foster R, Beech DJ, Bailey MA. ORAI1 Ca(2+) Channel as a Therapeutic Target in Pathological Vascular Remodelling. Front Cell Dev Biol. 2021; 9:653812. https://doi.org/10.3389/fcell.2021.653812 PMID: 33937254

37. Braun A, Varga-Szabo D, Kleinschnitz C, Pleines I, Bender M, Austinat M, et al. Orai1 (CRACM1) is the platelet SOC channel and essential for pathological thrombus formation. Blood. 2009; 113(9):2056–63. https://doi.org/10.1182/blood-2008-07-171611 PMID: 18832659

38. Authi KS. Orai1: a channel to safer antithrombotic therapy. Blood. 2009; 113(9):1872–3. https://doi.org/10.1182/blood-2008-11-185959 PMID: 19246564

39. Mammadova-Bach E, Nagy M, Heemskerk JWM, Nieswandt B, Braun A. Store-operated calcium entry in thrombosis and thrombo-inflammation. Cell Calcium. 2019; 77:39–48. https://doi.org/10.1016/j.ceca.2018.11.005 PMID: 30530092

40. van Kruchten R, Braun A, Feijge MA, Kuijpers MJ, Rivera-Galdos R, Kraft P, et al. Antithrombotic potential of blockers of store-operated calcium channels in platelets. Arterioscler Thromb Vasc Biol. 2012; 32(7):1717–23. https://doi.org/10.1161/ATVBAHA.111.243907 PMID: 22580895

41. Michelucci A, García-Castañeda M, Boncompagni S, Dirksen RT. Role of STIM1/ORAI1-mediated store-operated Ca(2+) entry in skeletal muscle physiology and disease. Cell Calcium. 2018; 76:101–15. https://doi.org/10.1016/j.ceca.2018.10.004 PMID: 30414508

42. Chen YF, Hsu KF, Shen MR. The store-operated Ca(2+) entry-mediated signaling is important for cancer spread. Biochim Biophys Acta. 2016; 1863(6 Pt B):1427–35. https://doi.org/10.1016/j.bbamcr.2015.11.030 PMID: 26643254

43. Jardin I, Rosado JA. STIM and calcium channel complexes in cancer. Biochim Biophys Acta. 2016; 1863(6 Pt B):1418–26. https://doi.org/10.1016/j.bbamcr.2015.10.003 PMID: 26455959

44. Villalobos C, Gutiérrez LG, Hernández-Morales M, Del Bosque D, Núñez L. Mitochondrial control of store-operated Ca(2+) channels in cancer: Pharmacological implications. Pharmacol Res. 2018; 135:136–43. https://doi.org/10.1016/j.phrs.2018.08.001 PMID: 30081178

45. Mei Y, Barrett JE, Hu H. Calcium release-activated calcium channels and pain. Cell Calcium. 2018; 74:180–5. https://doi.org/10.1016/j.ceca.2018.07.009 PMID: 30096536

46. Vigont V, Nekrasov E, Shalygin A, Gusev K, Klushnikov S, Illarioshkin S, et al. Patient-Specific iPSC-Based Models of Huntington's Disease as a Tool to Study Store-Operated Calcium Entry Drug Targeting. Front Pharmacol. 2018; 9:696. https://doi.org/10.3389/fphar.2018.00696 PMID: 30008670

47. Wu J, Shih HP, Vigont V, Hrdlicka L, Diggins L, Singh C, et al. Neuronal store-operated calcium entry pathway as a novel therapeutic target for Huntington's disease treatment. Chem Biol. 2011; 18(6):777–93. https://doi.org/10.1016/j.chembiol.2011.04.012 PMID: 21700213

48. Zhang H, Sun S, Wu L, Pchitskaya E, Zakharova O, Fon Tacer K, et al. Store-Operated Calcium Channel Complex in Postsynaptic Spines: A New Therapeutic Target for Alzheimer's Disease Treatment. J Neurosci. 2016; 36(47):11837–50. https://doi.org/10.1523/JNEUROSCI.1188-16.2016 PMID: 27881772

49. Ahuja M, Schwartz DM, Tandon M, Son A, Zeng M, Swaim W, et al. Orai1-Mediated Antimicrobial Secretion from Pancreatic Acini Shapes the Gut Microbiome and Regulates Gut Innate Immunity. Cell Metab. 2017; 25(3):635–46. https://doi.org/10.1016/j.cmet.2017.02.007 PMID: 28273482

50. Concepcion AR, Feske S. Regulation of epithelial ion transport in exocrine glands by store-operated Ca(2+) entry. Cell Calcium. 2017; 63:53–9. https://doi.org/10.1016/j.ceca.2016.12.004 PMID: 28027799

51. Liu H, Kabrah A, Ahuja M, Muallem S. CRAC channels in secretory epithelial cell function and disease. Cell Calcium. 2019; 78:48–55. https://doi.org/10.1016/j.ceca.2018.12.010 PMID: 30641249

52. Barde PJ, Viswanadha S, Veeraraghavan S, Vakkalanka SV, Nair A. A first-in-human study to evaluate the safety, tolerability and pharmacokinetics of RP3128, an oral calcium release-activated calcium (CRAC) channel modulator in healthy volunteers. J Clin Pharm Ther. 2021; 46(3):677–87. https://doi.org/10.1111/jcpt.13322 PMID: 33314326

53. Bruen C, Miller J, Wilburn J, Mackey C, Bollen TL, Stauderman K, et al. Auxora for the Treatment of Patients With Acute Pancreatitis and Accompanying Systemic Inflammatory Response Syndrome: Clinical Development of a Calcium Release-Activated Calcium Channel Inhibitor. Pancreas. 2021; 50(4):537–43. https://doi.org/10.1097/MPA.0000000000001793 PMID: 33939666

54. Miller J, Bruen C, Schnaus M, Zhang J, Ali S, Lind A, et al. Auxora versus standard of care for the treatment of severe or critical COVID-19 pneumonia: results from a randomized controlled trial. Crit Care. 2020; 24(1):502. https://doi.org/10.1186/s13054-020-03220-x PMID: 32795330

55. Bird GS, Putney J.W. Jr. Pharmacology of Store-Operated Calcum Entry Channels. In: Kozak JA, Putney J.W. Jr., editor. Calcium Entry Channels in Non-Excitable Cells. Boca Raton (FL): CRC Press/Taylor Francis; 2018. p. 311–24.

56. Jairaman A, Prakriya M. Molecular pharmacology of store-operated CRAC channels. Channels (Austin). 2013; 7(5):402–14. https://doi.org/10.4161/chan.25292 PMID: 23807116

57. Parekh AB. Store-operated CRAC channels: function in health and disease. Nat Rev Drug Discov. 2010; 9(5):399–410. https://doi.org/10.1038/nrd3136 PMID: 20395953

58. Stauderman KA. CRAC channels as targets for drug discovery and development. Cell Calcium. 2018; 74:147–59. https://doi.org/10.1016/j.ceca.2018.07.005 PMID: 30075400

59. Sweeney ZK, Minatti A, Button DC, Patrick S. Small-molecule inhibitors of store-operated calcium entry. ChemMedChem. 2009; 4(5):706–18. https://doi.org/10.1002/cmdc.200800452 PMID: 19330784

60. Grynkiewicz G, Poenie M, Tsien RY. A new generation of Ca2+ indicators with greatly improved fluorescence properties. J Biol Chem. 1985; 260(6):3440–50. PMID: 3838314

61. Johnson M. Calcium Imaging of Store-Operated Calcium (Ca(2+)) Entry (SOCE) in HEK293 Cells Using Fura-2. Methods Mol Biol. 2019; 1925:163–72. https://doi.org/10.1007/978-1-4939-9018-4_15 PMID: 30674026

62. Lytton J, Westlin M, Hanley MR. Thapsigargin inhibits the sarcoplasmic or endoplasmic reticulum Ca-ATPase family of calcium pumps. J Biol Chem. 1991; 266(26):17067–71. PMID: 1832668

63. Treiman M, Caspersen C, Christensen SB. A tool coming of age: thapsigargin as an inhibitor of sarco-endoplasmic reticulum Ca(2+)-ATPases. Trends Pharmacol Sci. 1998; 19(4):131–5. https://doi.org/10.1016/s0165-6147(98)01184-5 PMID: 9612087

64. Yoast RE, Emrich SM, Zhang X, Xin P, Johnson MT, Fike AJ, et al. The native ORAI channel trio underlies the diversity of Ca2+ signaling events. Nature Communications. 2020; 11(1):2444. https://doi.org/10.1038/s41467-020-16232-6 PMID: 32415068

65. Bokhobza A, Ziental-Gelus N, Allart L, Iamshanova O, Vanden Abeele F. Impact of SOCE Abolition by ORAI1 Knockout on the Proliferation, Adhesion, and Migration of HEK-293 Cells. Cells. 2021; 10(11). https://doi.org/10.3390/cells10113016 PMID: 34831241

66. Allen DG, Coe DM, Cooper AWJ, Gore PM, House D, Senger S, et al., N-Pyrazole Carboxamides as CRAC Channel Inhibitors patent WO/2010/122089. 2010.

67. Bernat JV, Rodriguez JG, Roig SG, Trias CE, Gispert LV, New Bicyclic Compounds as CRAC Channel Modulators patent EP2738172A1. 2012.

68. Li J, Cubbon RM, Wilson LA, Amer MS, McKeown L, Hou B, et al. Orai1 and CRAC channel dependence of VEGF-activated Ca2+ entry and endothelial tube formation. Circ Res. 2011; 108(10):1190–8. https://doi.org/10.1161/CIRCRESAHA.111.243352 PMID: 21441136

69. Li J, McKeown L, Ojelabi O, Stacey M, Foster R, O'Regan D, et al. Nanomolar potency and selectivity of a Ca^{2+} release-activated Ca^{2+} channel inhibitor against store-operated Ca^{2+} entry and migration of vascular smooth muscle cells. Br J Pharmacol. 2011; 164(2):382–93. https://doi.org/10.1111/j.1476-5381.2011.01368.x PMID: 21545575

70. Merritt JE, Armstrong WP, Benham CD, Hallam TJ, Jacob R, Jaxa-Chamiec A, et al. SK&F 96365, a novel inhibitor of receptor-mediated calcium entry. Biochem J. 1990; 271(2):515–22. https://doi.org/10.1042/bj2710515 PMID: 2173565

71. Schwarz G, Droogmans G, Nilius B. Multiple effects of SK&F 96365 on ionic currents and intracellular calcium in human endothelial cells. Cell Calcium. 1994; 15(1):45–54. https://doi.org/10.1016/0143-4160(94)90103-1 PMID: 7511989

72. Bencze M, Behuliak M, Vavřínová A, Zicha J. Broad-range TRP channel inhibitors (2-APB, flufenamic acid, SKF-96365) affect differently contraction of resistance and conduit femoral arteries of rat. Eur J Pharmacol. 2015; 765:533–40. https://doi.org/10.1016/j.ejphar.2015.09.014 PMID: 26384458

73. Zagranichnaya TK, Wu X, Villereal ML. Endogenous TRPC1, TRPC3, and TRPC7 proteins combine to form native store-operated channels in HEK-293 cells. J Biol Chem. 2005; 280(33):29559–69. https://doi.org/10.1074/jbc.M505842200 PMID: 15972814

74. Singh A, Hildebrand ME, Garcia E, Snutch TP. The transient receptor potential channel antagonist SKF96365 is a potent blocker of low-voltage-activated T-type calcium channels. Br J Pharmacol. 2010; 160(6):1464–75. https://doi.org/10.1111/j.1476-5381.2010.00786.x PMID: 20590636

75. Franzius D, Hoth M, Penner R. Non-specific effects of calcium entry antagonists in mast cells. Pflugers Arch. 1994; 428(5–6):433–8. https://doi.org/10.1007/BF00374562 PMID: 7838664

76. Chung SC, McDonald TV, Gardner P. Inhibition by SK&F 96365 of Ca2+ current, IL-2 production and activation in T lymphocytes. Br J Pharmacol. 1994; 113(3):861–8. https://doi.org/10.1111/j.1476-5381.1994.tb17072.x PMID: 7858878

77. Enfissi A, Prigent S, Colosetti P, Capiod T. The blocking of capacitative calcium entry by 2-aminoethyl diphenylborate (2-APB) and carboxyamidotriazole (CAI) inhibits proliferation in Hep G2 and Huh-7 human hepatoma cells. Cell Calcium. 2004; 36(6):459–67. https://doi.org/10.1016/j.ceca.2004.04.004 PMID: 15488595

78. Mignen O, Brink C, Enfissi A, Nadkarni A, Shuttleworth TJ, Giovannucci DR, et al. Carboxyamidotriazole-induced inhibition of mitochondrial calcium import blocks capacitative calcium entry and cell proliferation in HEK-293 cells. J Cell Sci. 2005; 118(Pt 23):5615–23. https://doi.org/10.1242/jcs.02663 PMID: 16306224

79. Maruyama T, Kanaji T, Nakade S, Kanno T, Mikoshiba K. 2APB, 2-aminoethoxydiphenyl borate, a membrane-penetrable modulator of Ins(1,4,5)P3-induced Ca2+ release. J Biochem. 1997; 122 (3):498–505. https://doi.org/10.1093/oxfordjournals.jbchem.a021780 PMID: 9348075

80. Prakriya M, Lewis RS. Potentiation and inhibition of Ca(2+) release-activated Ca(2+) channels by 2-aminoethyldiphenyl borate (2-APB) occurs independently of IP(3) receptors. J Physiol. 2001; 536(Pt 1):3–19. https://doi.org/10.1111/j.1469-7793.2001.t01-1-00003.x PMID: 11579153

81. Goto J, Suzuki AZ, Ozaki S, Matsumoto N, Nakamura T, Ebisui E, et al. Two novel 2-aminoethyl diphenylborinate (2-APB) analogues differentially activate and inhibit store-operated Ca(2+) entry via STIM proteins. Cell Calcium. 2010; 47(1):1–10. https://doi.org/10.1016/j.ceca.2009.10.004 PMID: 19945161

82. Djuric SW, BaMaung NY, Basha A, Liu H, Luly JR, Madar DJ, et al. 3,5-Bis(trifluoromethyl)pyrazoles: a novel class of NFAT transcription factor regulator. J Med Chem. 2000; 43(16):2975–81. https://doi.org/10.1021/jm990615a PMID: 10956206

83. Trevillyan JM, Chiou XG, Chen YW, Ballaron SJ, Sheets MP, Smith ML, et al. Potent inhibition of NFAT activation and T cell cytokine production by novel low molecular weight pyrazole compounds. J Biol Chem. 2001; 276(51):48118–26. https://doi.org/10.1074/jbc.M107919200 PMID: 11592964

84. Ishikawa J, Ohga K, Yoshino T, Takezawa R, Ichikawa A, Kubota H, et al. A pyrazole derivative, YM-58483, potently inhibits store-operated sustained Ca2+ influx and IL-2 production in T lymphocytes. J Immunol. 2003; 170(9):4441–9. https://doi.org/10.4049/jimmunol.170.9.4441 PMID: 12707319

85. Zitt C, Strauss B, Schwarz EC, Spaeth N, Rast G, Hatzelmann A, et al. Potent inhibition of Ca2+ release-activated Ca2+ channels and T-lymphocyte activation by the pyrazole derivative BTP2. J Biol Chem. 2004; 279(13):12427–37. https://doi.org/10.1074/jbc.M309297200 PMID: 14718545

86. Schleifer H, Doleschal B, Lichtenegger M, Oppenrieder R, Derler I, Frischauf I, et al. Novel pyrazole compounds for pharmacological discrimination between receptor-operated and store-operated Ca(2+) entry pathways. Br J Pharmacol. 2012; 167(8):1712–22. https://doi.org/10.1111/j.1476-5381.2012.02126.x PMID: 22862290

87. Xie TH M.; Mahiou H.; Ono M.; Sun l.; Chen S.; Zhang S.; et al, Method for Modulating Calcium Ion-Release-Activated Calcium Channels patent WO/2005/009954. 2005.

88. Ng SW, di Capite J, Singaravelu K, Parekh AB. Sustained activation of the tyrosine kinase Syk by antigen in mast cells requires local Ca2+ influx through Ca2+ release-activated Ca2+ channels. J Biol Chem. 2008; 283(46):31348–55. https://doi.org/10.1074/jbc.M804942200 PMID: 18806259

89. Bohnert JX Z.; Chen S.; Sun L., Compounds for Inflammation and Immune-Related Uses patent WO/2010/039236. 2010.

90. Chen G, Panicker S, Lau KY, Apparsundaram S, Patel VA, Chen SL, et al. Characterization of a novel CRAC inhibitor that potently blocks human T cell activation and effector functions. Mol Immunol. 2013; 54(3–4):355–67. https://doi.org/10.1016/j.molimm.2012.12.011 PMID: 23357789

91. Derler I, Schindl R, Fritsch R, Heftberger P, Riedl MC, Begg M, et al. The action of selective CRAC channel blockers is affected by the Orai pore geometry. Cell Calcium. 2013; 53(2):139–51. https://doi.org/10.1016/j.ceca.2012.11.005 PMID: 23218667

92. Rice LV, Bax HJ, Russell LJ, Barrett VJ, Walton SE, Deakin AM, et al. Characterization of selective Calcium-Release Activated Calcium channel blockers in mast cells and T-cells from human, rat, mouse and guinea-pig preparations. Eur J Pharmacol. 2013; 704(1–3):49–57. https://doi.org/10.1016/j.ejphar.2013.02.022 PMID: 23454522

93. Sadaghiani AM, Lee SM, Odegaard JI, Leveson-Gower DB, McPherson OM, Novick P, et al. Identification of Orai1 channel inhibitors by using minimal functional domains to screen small molecule microarrays. Chem Biol. 2014; 21(10):1278–92. https://doi.org/10.1016/j.chembiol.2014.08.016 PMID: 25308275

94. Harper JL, Camerini-Otero CS, Li AH, Kim SA, Jacobson KA, Daly JW. Dihydropyridines as inhibitors of capacitative calcium entry in leukemic HL-60 cells. Biochem Pharmacol. 2003; 65(3):329–38. https://doi.org/10.1016/s0006-2952(02)01488-0 PMID: 12527326

95. Esteve C, González J, Gual S, Vidal L, Alzina S, Sentellas S, et al. Discovery of 7-azaindole derivatives as potent Orai inhibitors showing efficacy in a preclinical model of asthma. Bioorg Med Chem Lett. 2015; 25(6):1217–22. https://doi.org/10.1016/j.bmcl.2015.01.063 PMID: 25690784

96. Velicelebi GS K.; Dunn M.; Roos J., Pancreatitis Treatment patent WO/2016/138472. 2016.

97. US National Library of Medicine Study of CM4620 to Reduce the Severity of Pancreatitis Due to Asparaginase Available online: https://clinicaltrials.gov/ct2/show/NCT04195347 (accessed on 30 Jan 2023). [Internet]. [cited 30 Jan 2023]. Available from: https://ClinicalTrials.gov/show/NCT04195347.

98. US National Library of Medicine CM4620 Injectable Emulsion Versus Supportive Care in Patients With Acute Pancreatitis and SIRS Available online: https://clinicaltrials.gov/ct2/show/NCT03401190

(accessed on 30 Jan 2023). [Internet]. https://ClinicalTrials.gov/show/NCT03401190. [cited 30 Jan 2023]. Available from: https://ClinicalTrials.gov/show/NCT04195347.

99. US National Library of Medicine a Study of Auxora in Patients With Acute Pancreatitis and Accompanying SIRS Available online: https://clinicaltrials.gov/ct2/show/NCT04681066 (accessed on 30 Jan 2023). [Internet]. [cited 30 Jan 2023]. Available from: https://ClinicalTrials.gov/show/NCT04681066.

100. Ramos S, Grigoryev S, Rogers E, Roos J, Whitten J, Stauderman K, et al. CM3457, a potent and selective oral CRAC channel inhibitor, suppresses T and mast cell function and is efficacious in rat models of arthritis and asthma (72.3). The Journal of Immunology. 2012; 188(1 Supplement):72.3–s.3.

101. Wen L, Voronina S, Javed MA, Awais M, Szatmary P, Latawiec D, et al. Inhibitors of ORAI1 Prevent Cytosolic Calcium-Associated Injury of Human Pancreatic Acinar Cells and Acute Pancreatitis in 3 Mouse Models. Gastroenterology. 2015; 149(2):481–92.e7. https://doi.org/10.1053/j.gastro.2015.04.015 PMID: 25917787

102. Rahman S, Rahman T. Unveiling some FDA-approved drugs as inhibitors of the store-operated Ca(2+) entry pathway. Sci Rep. 2017; 7(1):12881. https://doi.org/10.1038/s41598-017-13343-x PMID: 29038464

103. Jones PB, White DH. Reappraisal of the clinical use of leflunomide in rheumatoid arthritis and psoriatic arthritis. Open Access Rheumatol. 2010; 2:53–71. https://doi.org/10.2147/OARRR.S9448 PMID: 27789998

104. Garnock-Jones KP. Teriflunomide: a review of its use in relapsing multiple sclerosis. CNS Drugs. 2013; 27(12):1103–23. https://doi.org/10.1007/s40263-013-0118-2 PMID: 24198223

105. Masson B, Ribeuz HL, Sabourin J, Laubry L, Woodhouse E, Foster R, et al. Orai1 Inhibitors as Potential Treatments for Pulmonary Arterial Hypertension. Circulation Research. 2022; 131(9):e102–e19. https://doi.org/10.1161/CIRCRESAHA.122.321041 PMID: 36164973

106. Aussel C, Marhaba R, Pelassy C, Breittmayer JP. Submicromolar La3+ concentrations block the calcium release-activated channel, and impair CD69 and CD25 expression in CD3- or thapsigargin-activated Jurkat cells. Biochem J. 1996; 313 (Pt 3)(Pt 3):909–13. https://doi.org/10.1042/bj3130909 PMID: 8611174

107. Broad LM, Cannon TR, Taylor CW. A non-capacitative pathway activated by arachidonic acid is the major Ca2+ entry mechanism in rat A7r5 smooth muscle cells stimulated with low concentrations of vasopressin. J Physiol. 1999; 517 (Pt 1)(Pt 1):121–34. https://doi.org/10.1111/j.1469-7793.1999.0121z.x PMID: 10226154

108. Trebak M, Bird GS, McKay RR, Putney JW Jr. Comparison of human TRPC3 channels in receptor-activated and store-operated modes. Differential sensitivity to channel blockers suggests fundamental differences in channel composition. J Biol Chem. 2002; 277(24):21617–23. https://doi.org/10.1074/jbc.M202549200 PMID: 11943785

109. Bonnefond ML, Florent R, Lenoir S, Lambert B, Abeilard E, Giffard F, et al. Inhibition of store-operated channels by carboxyamidotriazole sensitizes ovarian carcinoma cells to anti-Bclx(L) strategies through Mcl-1 down-regulation. Oncotarget. 2018; 9(74):33896–911. https://doi.org/10.18632/oncotarget.26084 PMID: 30338034

110. Peinelt C, Lis A, Beck A, Fleig A, Penner R. 2-Aminoethoxydiphenyl borate directly facilitates and indirectly inhibits STIM1-dependent gating of CRAC channels. J Physiol. 2008; 586(13):3061–73. https://doi.org/10.1113/jphysiol.2008.151365 PMID: 18403424

111. Hofer A, Kovacs G, Zappatini A, Leuenberger M, Hediger MA, Lochner M. Design, synthesis and pharmacological characterization of analogs of 2-aminoethyl diphenylborinate (2-APB), a known store-operated calcium channel blocker, for inhibition of TRPV6-mediated calcium transport. Bioorg Med Chem. 2013; 21(11):3202–13. https://doi.org/10.1016/j.bmc.2013.03.037 PMID: 23602525

112. Lis A, Peinelt C, Beck A, Parvez S, Monteilh-Zoller M, Fleig A, et al. CRACM1, CRACM2, and CRACM3 are store-operated Ca2+ channels with distinct functional properties. Curr Biol. 2007; 17(9):794–800. https://doi.org/10.1016/j.cub.2007.03.065 PMID: 17442569

113. He LP, Hewavitharana T, Soboloff J, Spassova MA, Gill DL. A functional link between store-operated and TRPC channels revealed by the 3,5-bis(trifluoromethyl)pyrazole derivative, BTP2. J Biol Chem. 2005; 280(12):10997–1006. https://doi.org/10.1074/jbc.M411797200 PMID: 15647288

114. Takezawa R, Cheng H, Beck A, Ishikawa J, Launay P, Kubota H, et al. A pyrazole derivative potently inhibits lymphocyte Ca2+ influx and cytokine production by facilitating transient receptor potential melastatin 4 channel activity. Mol Pharmacol. 2006; 69(4):1413–20. https://doi.org/10.1124/mol.105.021154 PMID: 16407466

115. Glosse P, Feger M, Mutig K, Chen H, Hirche F, Hasan AA, et al. AMP-activated kinase is a regulator of fibroblast growth factor 23 production. Kidney Int. 2018; 94(3):491–501. https://doi.org/10.1016/j.kint.2018.03.006 PMID: 29861059

116. Liu X, Wan X, Kan H, Wang Y, Yu F, Feng L, et al. Hypoxia-induced upregulation of Orai1 drives colon cancer invasiveness and angiogenesis. Eur J Pharmacol. 2018; 832:1–10. https://doi.org/10.1016/j.ejphar.2018.05.008 PMID: 29753044

117. Zhang B, Naik JS, Jernigan NL, Walker BR, Resta TC. Reduced membrane cholesterol after chronic hypoxia limits Orai1-mediated pulmonary endothelial Ca(2+) entry. Am J Physiol Heart Circ Physiol. 2018; 314(2):H359–h69. https://doi.org/10.1152/ajpheart.00540.2017 PMID: 29101179

118. Rv Kruchten, Braun A, Feijge MAH, Kuijpers MJE, Rivera-Galdos R, Kraft P, et al. Antithrombotic Potential of Blockers of Store-Operated Calcium Channels in Platelets. Arteriosclerosis, Thrombosis, and Vascular Biology. 2012; 32(7):1717–23. https://doi.org/10.1161/ATVBAHA.111.243907 PMID: 22580895

119. Abdelazeem KNM, Droppova B, Sukkar B, al-Maghout T, Pelzl L, Zacharopoulou N, et al. Upregulation of Orai1 and STIM1 expression as well as store-operated Ca2+ entry in ovary carcinoma cells by placental growth factor. Biochemical and Biophysical Research Communications. 2019; 512(3):467–72. https://doi.org/10.1016/j.bbrc.2019.03.025 PMID: 30902388

120. Ma K, Liu P, Al-Maghout T, Sukkar B, Cao H, Voelkl J, et al. Phosphate-induced ORAI1 expression and store-operated Ca2+ entry in aortic smooth muscle cells. Journal of Molecular Medicine. 2019; 97 (10):1465–75. https://doi.org/10.1007/s00109-019-01824-7 PMID: 31385016

121. Zhu X, Ma K, Zhou K, Liu J, Nürnberg B, Lang F. Vasopressin-stimulated ORAI1 expression and store-operated Ca2+ entry in aortic smooth muscle cells. Journal of Molecular Medicine. 2021; 99 (3):373–82. https://doi.org/10.1007/s00109-020-02016-4 PMID: 33409552

122. Hendron E, Wang X, Zhou Y, Cai X, Goto J, Mikoshiba K, et al. Potent functional uncoupling between STIM1 and Orai1 by dimeric 2-aminodiphenyl borinate analogs. Cell Calcium. 2014; 56(6):482–92. https://doi.org/10.1016/j.ceca.2014.10.005 PMID: 25459299

123. Yeromin AV, Roos J, Stauderman KA, Cahalan MD. A store-operated calcium channel in Drosophila S2 cells. J Gen Physiol. 2004; 123(2):167–82. https://doi.org/10.1085/jgp.200308982 PMID: 14744989

124. McNally BA, Yamashita M, Engh A, Prakriya M. Structural determinants of ion permeation in CRAC channels. Proc Natl Acad Sci U S A. 2009; 106(52):22516–21. https://doi.org/10.1073/pnas.0909574106 PMID: 20018736

125. Pałasz A, Czekaj P. Toxicological and cytophysiological aspects of lanthanides action. Acta Biochim Pol. 2000; 47(4):1107–14. PMID: 11996100

126. Gross SA, Wissenbach U, Philipp SE, Freichel M, Cavalié A, Flockerzi V. Murine ORAI2 splice variants form functional Ca2+ release-activated Ca2+ (CRAC) channels. J Biol Chem. 2007; 282 (27):19375–84. https://doi.org/10.1074/jbc.M701962200 PMID: 17463004

127. Obergrussberger A, Goetze TA, Brinkwirth N, Becker N, Friis S, Rapedius M, et al. An update on the advancing high-throughput screening techniques for patch clamp-based ion channel screens: implications for drug discovery. Expert Opin Drug Discov. 2018; 13(3):269–77. https://doi.org/10.1080/17460441.2018.1428555 PMID: 29343120